



TECHNICAL ARTICLE

# Kinetic and Thermodynamic Studies on Lead-Rich Slag Reduction at Various CaO/SiO<sub>2</sub> Ratios

SUI XIE,<sup>1</sup> CHUNFA LIAO,<sup>1</sup> and BAOJUN ZHAO<sup>1,2,3</sup>

1.—Faculty of Materials Metallurgy and Chemistry, Jiangxi University of Science and Technology, Ganzhou, China. 2.—Sustainable Minerals Institute, University of Queensland, Brisbane, Australia. 3.—e-mail: bzhao@jxust.edu.cn

A bath smelting furnace is a clean technology replacing sinter machines to simultaneously produce lead-rich slag and lead metal. Lead-rich slag can be used as a feedstock for blast furnaces or smelting reduction furnaces to produce lead metal. Understanding the reduction mechanism of lead-rich slag by carbon provides useful information for the complete reduction of the lead oxide. Kinetic studies on the reduction of lead-rich slags with CaO/SiO<sub>2</sub> ratios of 0.38, 0.56, and 0.80 were carried out in the temperature range 1073–1473 K. The volume of the product gas was measured continuously to represent the extent of lead-rich slag reduction. It was found that the reduction was initially chemically controlled and then diffusion controlled. At the chemically-controlled stage, the activation energy of the reduction was higher at lower CaO/SiO<sub>2</sub> ratios. An increase of the CaO/SiO<sub>2</sub> ratio from 0.38 to 0.56 can decrease the activation energy from 273 kJ/mol to 95 kJ/mol. At the diffusion-controlled stage, the activation energy was determined to be 392 kJ/mol, 294 kJ/mol, and 280 kJ/mol for the slags with CaO/SiO<sub>2</sub> ratios of 0.38, 0.56, and 0.80, respectively. Formation of liquid plays an important role in the reduction of the lead-rich slag. The reduction mechanism has been analyzed by experimental results and thermodynamic calculations.

## INTRODUCTION

Lead is an important metal in modern industry due to its excellent ductility, corrosion resistance, and low electrical conductivity. It is widely used in metallurgy, radiation protection, and chemical power sources.<sup>1,2</sup> China produced 1.9 million tons of lead in 2020, which is four times as much as the second-largest producer, Australia (0.48 million tons).<sup>3</sup> Sintering-furnace has been a traditional process to produce lead metal, but has the disadvantages of low SO<sub>2</sub> utilization, high lead fugitive emissions, and expensive coke consumption. Several new lead production technologies, including TSL, QSL, Kaldor, and Kivcet, have been developed, but they have not been extensively applied in China due to high capital investment and unsatisfactory feedback from industry.<sup>4</sup> The Yunan Metallurgical

Group introduced the ISA process to simultaneously produce lead-rich slag and lead metal. The lead-rich slag was reduced in a blast furnace to obtain lead metal.<sup>5</sup> The Shuikoushan (SKS) process has been developed in recent years, and has become a mainstream lead-smelting process, with approximately 80% of lead production in China.<sup>6–8</sup> The new technology has a high automation degree, friendly operating environment, high production capacity, low waste emissions, and high SO<sub>2</sub> concentration and utilization. In the SKS process, an oxygen-rich bottom blow furnace is used for smelting oxidation to produce lead metal and lead-rich slag. A second oxygen-rich bottom blow furnace is used for smelting reduction to produce lead metal from the lead-rich slag.

Lead-rich slag is produced from liquid which has different properties from the sinter. It is important to understand the reduction mechanisms and kinetics of lead-rich slag in order to optimize the reduction operations. Upashya<sup>9</sup> found that the reduction of PbO in a liquid slag by carbon in iron contained

(Received February 25, 2022; accepted June 29, 2022; published online July 13, 2022)

two stages, a chemically-controlled stage and a diffusion-controlled stage. Kinaev et al.<sup>10</sup> compared the reduction kinetics of lead-smelting slag by graphite and coke. They reported that the reaction rates were almost independent of carbon reactivity, CaO/SiO<sub>2</sub>, and the SiO<sub>2</sub>/Fe ratio. Zhao et al.<sup>11</sup> compared the reduction characteristics of synthetic lead-rich slag and industrial lead sinters by CO gas. It has been shown that the extent of reduction of dense slag is equivalent to those achieved with conventional sinters. Rapid reduction is associated with increased proportions of liquid phase in both sinter and slag. Hou et al.<sup>12</sup> reported the reduction kinetics of lead sinter and synthetic lead slag by carbon at 1073–1473 K. They found that the formation of liquid was essential in order to have a rapid reduction reaction, and that the liquid proportion was influenced by the compositions of the sinter and slag. Liao et al.<sup>13</sup> investigated the phase equilibria of the system PbO–“FeOx”–CaO–SiO<sub>2</sub>–ZnO–Al<sub>2</sub>O<sub>3</sub> to characterize lead-rich slag. They found that the liquidus temperatures of the lead-rich slags were determined by their bulk compositions. It was reported that the basicity (CaO/SiO<sub>2</sub>) of the TiO<sub>2</sub>-bearing slag is one of the important parameters affecting its viscosity.<sup>14</sup> However, little work has been reported on the reduction kinetics of lead-rich slag at different CaO/SiO<sub>2</sub> ratios.

This study aims to investigate the effect of CaO/SiO<sub>2</sub> ratios on the reduction mechanisms and kinetics of lead-rich slags. The reducibility of the lead-rich slags is examined by experimental measurements and thermodynamic analysis.<sup>15</sup> The reduction kinetics of lead-rich slag with various CaO/SiO<sub>2</sub> are discussed using the shrinking core model.<sup>16–19</sup>

## RESEARCH METHODOLOGY

### Preparation and Characterization of Lead-Rich Slag

Typical compositions of some industrial lead-rich slags are given in Table I, from which it can be seen that the PbO concentration of these slags ranged from 33.3 to 58.1 wt.%, while the CaO/SiO<sub>2</sub> ratio ranged from 0.33 to 0.69.

The lead-rich slags used in the present study were selected based on industrial slags and prepared by melting pure PbO, ZnO, Fe<sub>2</sub>O<sub>3</sub>, CaCO<sub>3</sub>, and SiO<sub>2</sub>

powders in corundum crucibles in an induction furnace. The bulk compositions of the slow-cooled lead-rich slags were measured by XRF, as shown in Table II. The PbO, ZnO, and Fe<sub>2</sub>O<sub>3</sub> concentrations are approximately the same in the three samples (labeled Y1, Y2, and Y3), and the CaO/SiO<sub>2</sub> ratios are 0.38, 0.56, and 0.8 for Y1, Y2, and Y3, respectively. The lead-rich slags were mounted in epoxy resin, polished, and examined using optical and scanning electron microscopy. A JEOL 8800L electron probe microanalyzer with a wavelength-dispersive spectrometer (WDS) was employed to measure the compositions of the phases present in the slags. An accelerating voltage of 15 kV and a probe current of 15 nA were applied. The average accuracy of the EPMA measurements is within 1 wt.%.

The typical microstructures of Y2 have been reported previously<sup>12</sup> while the typical microstructures of Y1 and Y3 are shown in Fig. 1. It can be seen that in the slow-cooled samples, glass, spinel, and melilite are the major phases present in both samples. The proportion and sizes of the solid phases in Y3 are higher than those in Y1. Some lead-containing silicates, such as Pb-Ca silicates (PCS) and Pb-Fe silicates (PFS) are also observed in Y1 and Y3, respectively. Slightly different phase assembles in the sample indicated different cooling rates of the sample. Figure 1a shows the sample located on the surface or close to the crucible wall which had a fast cooling rate.

### Reduction of Lead-Rich Slag

The equipment used in this study is shown in Fig. 2. The reduction experiments were carried out in graphite crucibles (18 mm OD, 14 mm ID, and 40 mm high) which were placed in a corundum reaction tube (19 mm ID) and heated in a vertical furnace. A Pt/Pt-13%Rh thermocouple inside an alumina sheath supported the graphite crucibles held on the hot zone of the furnace. The exit port of the off-gas was connected to a water-containing pressure device, which captured the gas generated from the reduction reaction, and displaced the same volume of water into a container sitting on a balance. The balance was connected to a computer to continuously record the weight changes.

The graphite crucible placed on the platform was slowly raised into the hot zone of the furnace after 30 min of flushing by ultrahigh purity argon. The

**Table I. Typical compositions of industrial lead-rich slags (wt%)**

References	PbO	ZnO	Fe <sub>2</sub> O <sub>3</sub>	CaO	SiO <sub>2</sub>	Al <sub>2</sub> O <sub>3</sub>	CaO/SiO <sub>2</sub>
He et al. <sup>20</sup>	58.13	8.04	12.34	3.07	8.31	1.78	0.37
Liu et al. <sup>21</sup>	42.75	14.22	16.15	5.30	7.65	–	0.69
Pi et al. <sup>22</sup>	37.03	17.60	20.27	4.81	14.35	–	0.33
	33.34	19.70	17.44	4.59	13.71	–	0.33
	54.10	1.20	16.15	3.74	8.14	–	0.47
Wang et al. <sup>23</sup>	46.96	12.89	16.32	4.31	7.88	1.05	0.54

**Table II. Compositions of the lead-rich slags for reduction experiments**

Sample	CaO/SiO <sub>2</sub>	PbO	ZnO	Fe <sub>2</sub> O <sub>3</sub>	CaO	SiO <sub>2</sub>	Al <sub>2</sub> O <sub>3</sub>
Y1	0.38	49	10.7	16.1	6.3	16.6	1.2
Y2	0.56	51.8	11.4	17.0	6.7	11.9	1.3
Y3	0.8	50.4	11.1	16.5	9.2	11.5	1.3

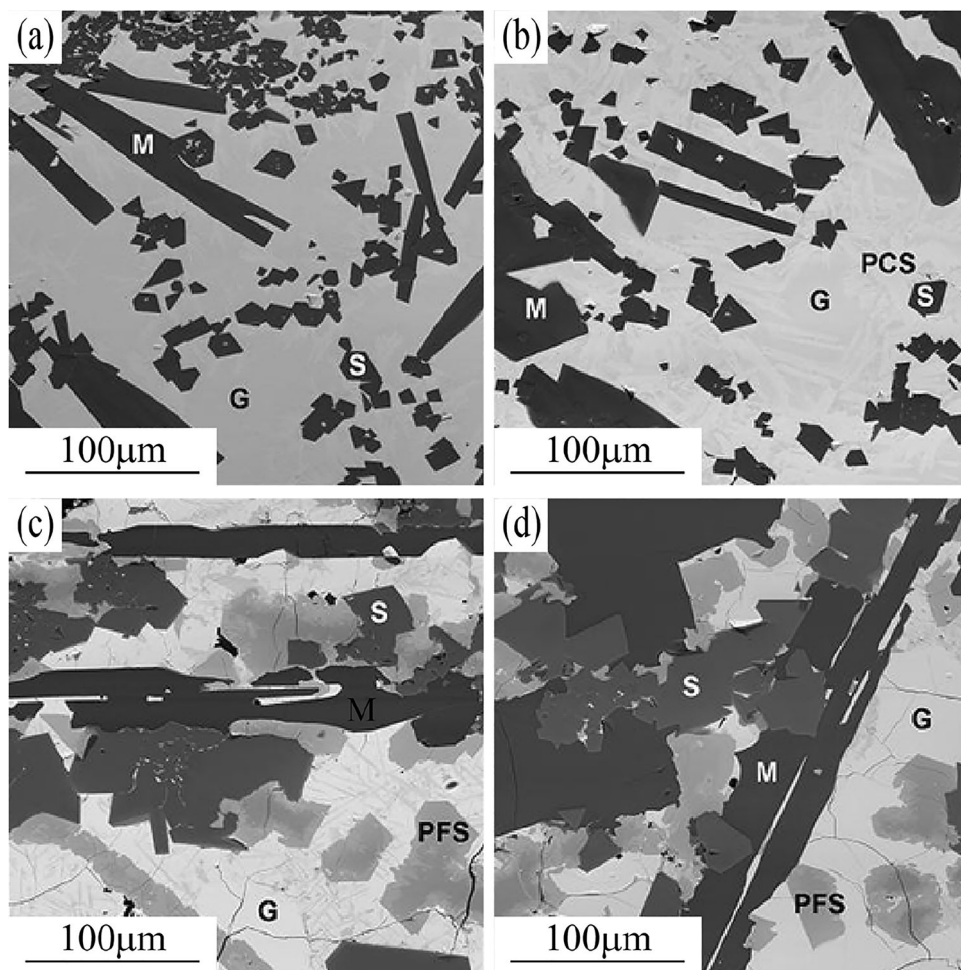


Fig. 1. Typical microstructures of slow-cooled lead-rich slags: Y1(a, b) and Y3(c, d); G glass, M melilite, S spinel, Pb lead metal, PFS lead-iron silicate, PCS lead calcium silicate.

gas flushing was then stopped, and the reaction tube was sealed. The argon gas was turned on carefully to enable the water to stay at point A indicated in Fig. 2, and then the argon gas was stopped. The balance was adjusted to zero and the program on the computer was started to record the data. A 5.00-g lead-rich slag sample of approximately 1 mm diameter was added to the graphite crucible from the top of furnace. Once the slag sample touched the graphite crucible, the reduction reaction started, and CO/CO<sub>2</sub> gases were generated and captured in a water-containing pressure device, which was led to the displacement of water into a container on a balance (accuracy 0.001 g). The volume of CO/CO<sub>2</sub> gases was continuously recorded

every 5 s by determining the weight of the water. Up to 400 ml of CO/CO<sub>2</sub> gases (approximately 400 g H<sub>2</sub>O) can be generated during the reduction of 5 g of lead-rich slag. When the graphite crucible was lowered from the hot zone and cooled to room temperature under Ar gas flow, the reduction reaction was stopped. The product gas was the mixture of CO and CO<sub>2</sub> during the reduction. The composition of the gas mixture was not analyzed. The total gas volume was used to represent the extent of the reduction.

### Thermodynamic Calculations

The thermodynamic software, FactSage 8.1, was used to predict the proportions of the phases and the

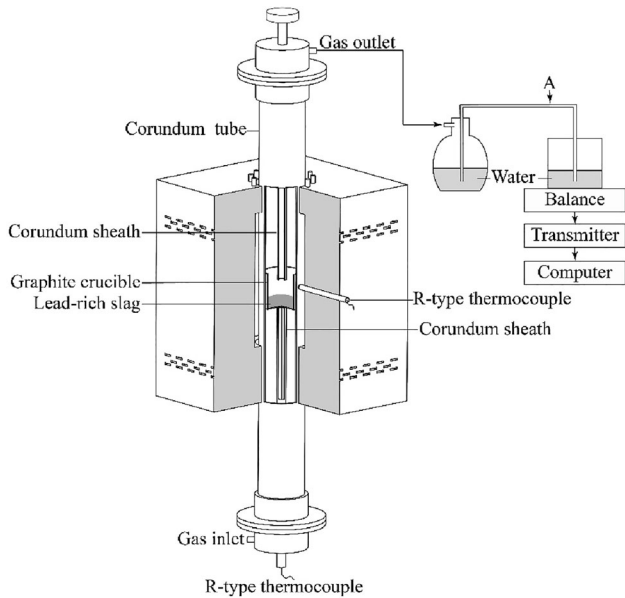


Fig. 2. Assembly of the vertical furnace, gas collection, and data recording system used in this study.

viscosity of the liquid slags at high temperature.<sup>15</sup> The activities of ZnO and PbO in the slags were also calculated using FactSage. The databases selected were “FactPs” and “Ftoxiide”. The solution phases selected in the calculations were “FToxid-SLAGA”, “FToxid-SPINA”, “FToxid-MeO”, “FToxid-cPyrA”, “FToxid-PyrA”, “FToxid-WOLLA”, “FToxid-Bred”, “FToxid-bC2SA”, “FToxid-aC2SA”, “FToxid-Mel”, “FToxid-Oliv”, “FToxid-Mull”, “FToxid-CORU”, “FToxid-ZNIT”, “FToxid-WILL”, “FToxid-PbO”, and “FToxid-PCSi”.

## RESULTS AND DISCUSSION

### Reduction of Lead-Rich Slag by Carbon

When carbon reacts with liquid slag containing  $\text{Fe}_2\text{O}_3$ , PbO, and ZnO, the reactions below may occur:

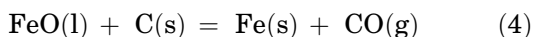
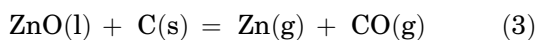
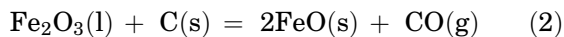
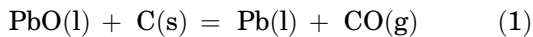


Figure 3 shows the extent of Eqs. (1–4) at 1473 K for Y2 calculated by FactSage. The reduction of  $\text{Fe}_2\text{O}_3$  to FeO starts first and is followed by the reduction of PbO to Pb. When Eqs. (1) and (2) are almost complete, the reduction of ZnO to Zn begins. Metallic iron was not observed in the sample after the reduction, indicating that Eq. (4) did not occur in the temperature range investigated.

The reducibility is calculated according to:

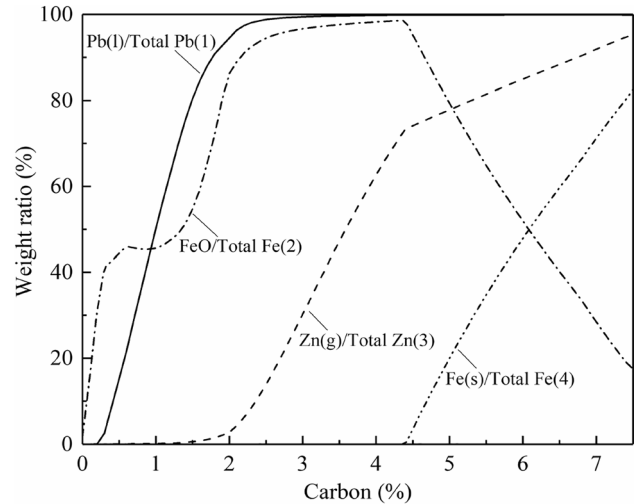


Fig. 3. Extents of reactions (1–4) at 1473 K in Y2.

$$\alpha = V_m \times 100\% / V_T \quad (5)$$

where  $V_m$  is the experimentally measured gas volume (ml),  $V_T$  is the total volume of the theoretical gas generated from Eqs. (1, 2 and 3) (ml) by 5 g slag, and  $\alpha$  is the reducibility (%).

Figure 4 shows the reducibility of Y1 ( $\text{CaO}/\text{SiO}_2 = 0.38$ ) and Y3 ( $\text{CaO}/\text{SiO}_2 = 0.80$ ) as a function of reaction time at 1073, 1173, 1273, 1373, and 1473 K. It can be seen from Fig. 4 that the reduction of lead-rich slag includes two stages, as reported by Upashya.<sup>9</sup> At the beginning of the reduction, the reaction was chemically controlled, and the reducibility increased rapidly with time. With the progress of the reduction, the reaction was controlled by diffusion. The reducibility increases slowly with time at this stage. Temperature has a significant influence on the reducibility. In the case of Y1, the reaction between the lead-rich slag and carbon was limited at temperatures below 1273 K. In the case of Y3, the reaction between the lead-rich slag and carbon was limited at temperatures below 1173 K. It is clear that the reducibility of Y3 is always higher than that of Y1 at the same temperature, indicating the  $\text{CaO}/\text{SiO}_2$  ratio has a significant effect on the reducibility of the lead-rich slag.

The effects of the temperature and  $\text{CaO}/\text{SiO}_2$  ratio on reducibility are shown in Fig. 5. Figure 5a and b shows the reducibility of three slags at 200- and 3500-s reduction to represent the reactions at the chemically-controlled stage and the diffusion-controlled stage, respectively. It can be seen that, in both stages, the reducibility always increases slowly at low temperatures and rapidly at high temperatures. Slag Y2 ( $\text{CaO}/\text{SiO}_2 = 0.56$ ) and Y3 ( $\text{CaO}/\text{SiO}_2 = 0.80$ ) have similar reducibility, but always higher than that of Y1 ( $\text{CaO}/\text{SiO}_2 = 0.38$ ). It seems that a critical  $\text{CaO}/\text{SiO}_2$  ratio is required between 0.38 and 0.56 to promote the reduction of the lead-rich slag. Higher  $\text{CaO}/\text{SiO}_2$  ratios than 0.56, which

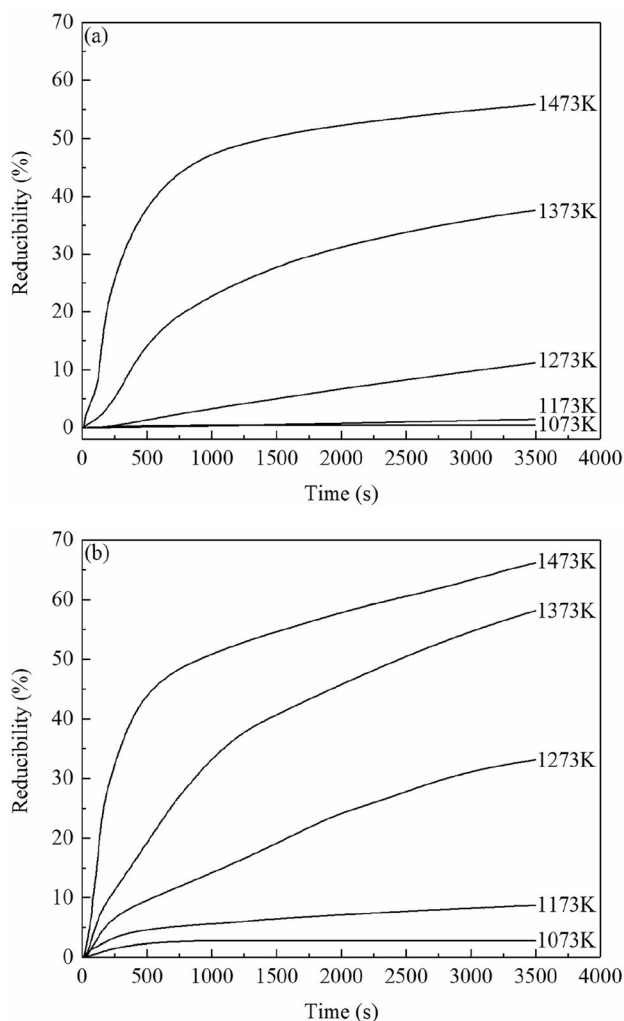


Fig. 4. Reducibility as a function of reaction time: (a) Y1, CaO/SiO<sub>2</sub> = 0.38, (b) Y3, CaO/SiO<sub>2</sub> = 0.8.

can only increase the flux cost and slag volume are not necessary.

The typical microstructures of Y1 and Y3 after the reductions at 1173 K and 1373 K are shown in Fig. 6. These microstructures do not represent the phase assemblages at high temperatures, as the slags were not quenched after the reduction. As shown in the figure, glass, spinel, and melilite are the major phases present in all the samples which is similar to the microstructures of the lead-rich slag before reduction. In addition, metallic lead is observed in all the samples, indicating the reduction of PbO to Pb occurred in these experiments.

### Reduction Kinetics

It can be seen from Fig. 4 that the reduction of lead-rich slag includes two stages, the chemically-controlled stage at the initial reactions and the diffusion-controlled stage at the further reactions. The reduction Eqs. (1, 2, 3 and 4) are mainly liquid-

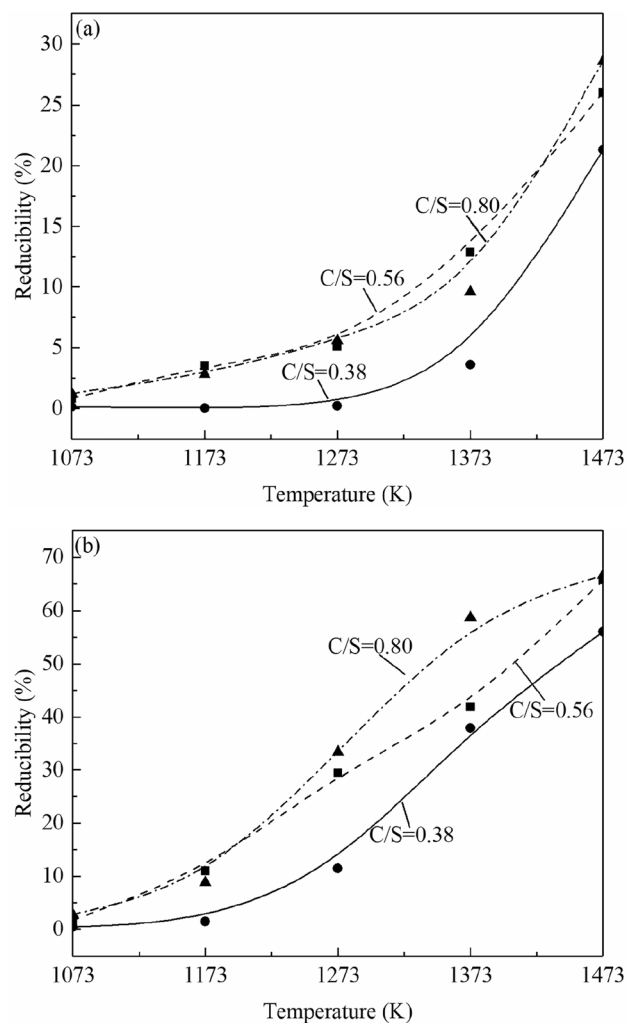


Fig. 5. Comparison of the reducibility of three slags: (a) after 200 s reaction, (b) after 3500 s reaction.

solid reactions and the shrinking-core model is often applied to analyze the reaction kinetics. The experimental results of the lead-rich slag reductions have been analyzed in two steps.

- (1) The reducibility of the reduction reaction can be calculated as a function of time at a fixed temperature. In the chemically-controlled stage, the equation can be expressed as:<sup>16-19</sup>

$$1 - (1 - \alpha)^{1/3} = kt \quad (6)$$

where  $\alpha$  is the reducibility,  $t$  is the reaction time, and  $k$  is the reaction rate constant. It can be seen from supplementary Figure S1(a) (refer to online supplementary material) that this equation was found to be able to simulate the experimental results in the chemically-controlled stage, as shown in Fig. 4. The reaction rate constant can be obtained for each experiment at a given temperature. In the diffusion-controlled stage, various reaction models have been proposed. It can be seen from

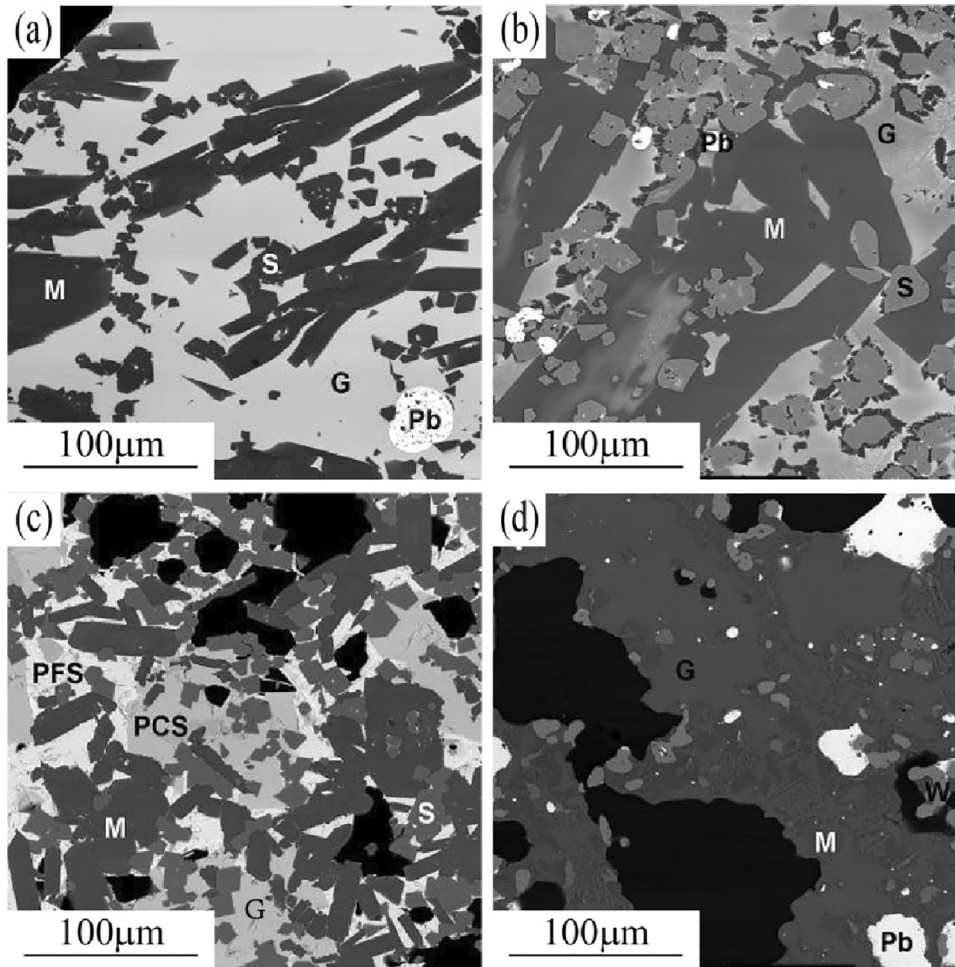


Fig. 6. Typical microstructures of the reduced slag: (a) Y1 1173 K; (b) Y1 1373 K; (c) Y3 1173 K; (d) Y3 1373 K; G glass, M melilite, S spinel, Pb lead metal, PFS lead-iron silicate, PCS lead calcium silicate.

supplementary Figure S1b that the one suggested by Dickinson<sup>16</sup> provided the best fit to the experimental data shown in Fig. 4 to describe the reduction in the diffusion-controlled stage:

$$\left[(1-\alpha)^{-1/3}-1\right]^2 = kt \quad (7)$$

Similarly, the reaction rate constant in the diffusion-controlled stage can be obtained for each experiment at a given temperature. The reaction rate constants from the experimental data are given in Table III.

- (2) According to the Arrhenius equation, the reaction rate constant as a function of temperature can be expressed as:

$$k = Ae^{-E/RT} \quad (8)$$

where  $A$  is the pre-exponential factor ( $s^{-1}$ ),  $E$  is the activation energy ( $J \cdot mol^{-1}$ ),  $R$  is the gas constant ( $8.314 J \cdot mol^{-1} K^{-1}$ ), and  $T$  is the absolute temperature (K). Equation (9) can be rewritten as:

$$\ln(k) = -\frac{E}{RT} + A \quad (9)$$

Therefore, the activation energy can be obtained from a linear relationship between  $\ln(k)$  and  $1/T$ . Figure 7a and b shows the relationships between  $\ln(k)$  and  $1/T$  in the chemically-controlled stage and the diffusion-controlled stage, respectively. It can be seen from Fig. 7a that the slopes of Y2 ( $CaO/SiO_2 = 0.56$ ) and Y3 ( $CaO/SiO_2 = 0.80$ ) are close, and that they are significantly different from that of Y1 ( $CaO/SiO_2 = 0.38$ ). The activation energies of Y1, Y2, and Y3, at the chemically-controlled stage, are 273 kJ/mol, 95 kJ/mol, and 100 kJ/mol, respectively. This again confirms the results shown in Fig. 5 that a critical  $CaO/SiO_2$  ratio is present between 0.38 and 0.56 to decrease the activation energy at the chemically-controlled stage. Similarly, it can be seen from Fig. 7b that, at the diffusion-controlled stage, the activation energies of Y1, Y2, and Y3 are 392 kJ/mol, 294 kJ/mol, and 280 kJ/mol, respectively. The increase of the  $CaO/SiO_2$  ratio,

**Table III. Experimentally determined reaction rate constants**

	Chemically-controlled stage					Diffusion-controlled stage				
	1073 K	1173 K	1273 K	1373 K	1473 K	1073 K	1173 K	1273 K	1373 K	1473 K
Y1	—	$1.2 \times 10^{-6}$	$9.4 \times 10^{-6}$	$5.0 \times 10^{-5}$	$4.0 \times 10^{-4}$	$1.3 \times 10^{-10}$	$1.3 \times 10^{-8}$	$8.4 \times 10^{-7}$	$6.8 \times 10^{-6}$	$1.2 \times 10^{-5}$
Y2	$3.8 \times 10^{-5}$	$3.9 \times 10^{-5}$	$1.2 \times 10^{-4}$	$3.1 \times 10^{-4}$	$5.3 \times 10^{-4}$	$3.6 \times 10^{-9}$	$4.3 \times 10^{-7}$	$5.1 \times 10^{-6}$	$9.8 \times 10^{-6}$	$4.0 \times 10^{-5}$
Y3	$2.4 \times 10^{-5}$	$7.7 \times 10^{-5}$	$1.1 \times 10^{-4}$	$2.3 \times 10^{-4}$	$6.5 \times 10^{-4}$	—	$2.1 \times 10^{-7}$	$5.1 \times 10^{-6}$	$4.5 \times 10^{-5}$	$6.2 \times 10^{-5}$

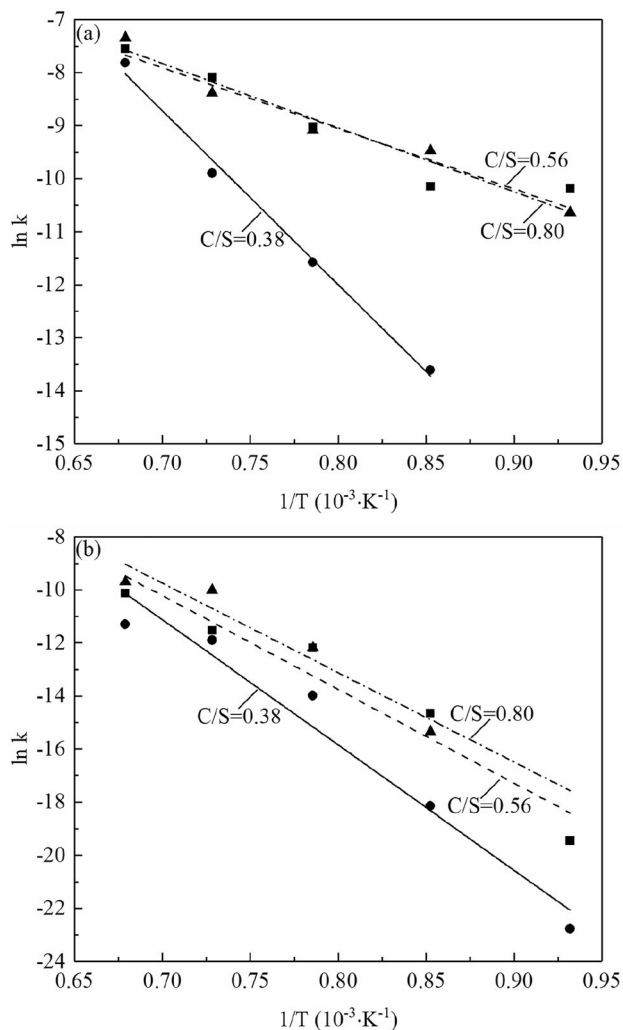


Fig. 7. The relationship between  $\ln(k)$  and  $1/T$  for the reduction reactions of Y1 ( $\text{CaO/SiO}_2 = 0.38$ ), Y2 ( $\text{CaO/SiO}_2 = 0.56$ ), and Y3 ( $\text{CaO/SiO}_2 = 0.80$ ): at the chemically controlled stage, and (b) at the diffusion-controlled stage.

from 0.38 to 0.56, significantly decreases the activation energy, from 392 kJ/mol to 294 kJ/mol. A further increase of the CaO/SiO<sub>2</sub> ratio, from 0.56 to 0.80, only slightly decreases the activation energy, from 294 kJ/mol to 280 kJ/mol. In conclusion, an increase of CaO/SiO<sub>2</sub> ratio in the lead-rich slags is favorable for increasing the reaction rate in both the

chemically-controlled stage and the diffusion-controlled stage, while the increase of the reaction rate is not significant if the CaO/SiO<sub>2</sub> ratio in the lead-rich slag is higher than 0.56.

### Thermodynamic Analysis

High-temperature reactions are fast and approach equilibrium. Thermodynamic analysis is used to understand and explain the reaction kinetics of lead-rich slag reduction. To understand the properties of the slags at different stages of the reduction, the proportion of liquid, liquid viscosity, and activities of PbO and ZnO in the liquid have been calculated from FactSage.<sup>15</sup> Figure 8 shows the proportions and viscosities of liquid slags formed at different temperatures for the lead-rich slags Y1, Y2, and Y3. The properties of the lead-rich slags are directly related to the chemically-controlled reduction. It can be seen from Fig. 8a that, at low temperatures, the proportion of the liquid slag increases rapidly with increasing temperature. Approximately 60% liquid is formed at 1173 K. Between 1073 K and 1173 K, the slag with a higher CaO/SiO<sub>2</sub> ratio can form more liquid. This confirms the experimental results shown in Figs. 4 and 5a where Y3 has a higher reducibility than Y1 at 1073 K and 1173 K. On the other hand, it can be seen from Fig. 8a that, between 1223 K and 1423 K, the proportions of the liquid in the three slags are all in the range of 60–85%, and the proportion of the liquid is higher in Y1 than those of Y2 and Y3. This indicates that, when liquid is present as the major component, the proportion of the liquid is no longer the main factor influencing the reaction rate. It can be seen from Fig. 8b that the liquid formed in Y1 always has a much higher viscosity than Y2 and Y3 in the investigated temperature range. As the CaO/SiO<sub>2</sub> ratio in the slag increases, more Ca<sup>2+</sup> in the silicate liquid breaks the long -O-Si-O- chain and the viscosity of the liquid slag is reduced. The chemical reaction between carbon and the low-viscosity liquid was therefore accelerated<sup>24</sup>. Figure 9 shows the activities of PbO and ZnO in the liquid formed in Y1, Y2, and Y3, respectively. It can be seen that the activity of PbO decreases and the activity of ZnO increases with increasing temperature. The reason is that the dissolution of the ZnO-

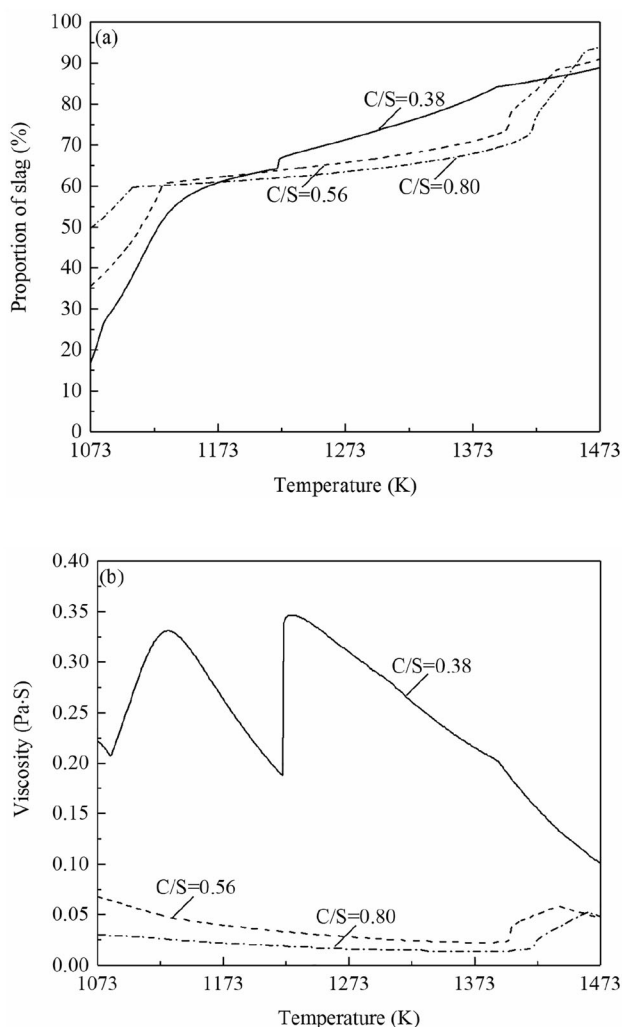


Fig. 8. The proportions and viscosities of liquid slags at different temperatures for Y1 ( $\text{CaO}/\text{SiO}_2 = 0.38$ ), Y2 ( $\text{CaO}/\text{SiO}_2 = 0.56$ ), and Y3 ( $\text{CaO}/\text{SiO}_2 = 0.80$ ): (a) proportion, (b) viscosity.

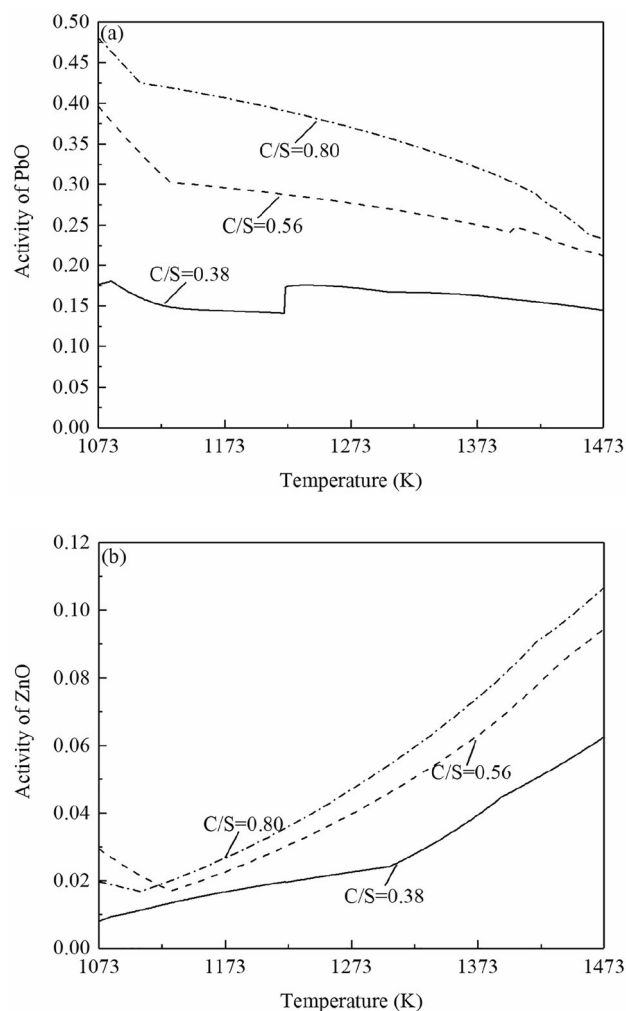


Fig. 9. The activities of PbO and ZnO in lead-rich slags at different temperatures for Y1 ( $\text{CaO}/\text{SiO}_2 = 0.38$ ), Y2 ( $\text{CaO}/\text{SiO}_2 = 0.56$ ), and Y3 ( $\text{CaO}/\text{SiO}_2 = 0.80$ ): (a) PbO, (b) ZnO.

containing phases, such as melilite and spinel into the liquid, results in higher concentrations of ZnO and lower concentrations of PbO. It can be seen from Fig. 9 that the activities of PbO and ZnO in the liquid increase with increasing  $\text{CaO}/\text{SiO}_2$  ratio in the slag. Y2 and Y3 as a group have much higher activities of PbO and ZnO in the liquid than Y1. The trends of the activities of PbO and ZnO in the liquid, together with the liquid viscosity, can well explain the reducibility of the lead-rich slags at high temperatures.

## CONCLUSION

The reduction kinetics of lead-rich slag have been investigated by accurate measurements of the gas volume generated from the reactions. The reduction of the lead-rich slag by carbon was chemically controlled at the beginning and then diffusion controlled. The activation energies at the chemically-controlled and the diffusion-controlled stages have been determined based on the experimental

data. The proportion and viscosity of the liquid slag and the activities of ZnO and PbO in the slag have been calculated using FactSage 8.1 to explain the reduction mechanisms. The results showed that:

- (1) The reduction of PbO and  $\text{Fe}_2\text{O}_3$  can happen concurrently, followed by the reduction of ZnO. Reduction of FeO by C was not observed under the experimental conditions.
- (2) The reduction of lead-rich slag at different  $\text{CaO}/\text{SiO}_2$  ratios was initially fast but becomes slower as the reducibility increases. The reducibility markedly increases at temperatures above 1173 K where significant amounts of liquid are formed.
- (3) The activation energy of the lead-rich slag reduction at  $\text{CaO}/\text{SiO}_2 = 0.38$ , 0.56, and 0.80 at the chemically-controlled stage is 273 kJ/mol, 95 kJ/mol, and 100 kJ/mol respectively. The activation energy at the diffusion-controlled stage is 392 kJ/mol, 294 kJ/mol, and 280 kJ/mol, respectively. The activation



energy decreases sharply when the CaO/SiO<sub>2</sub> ratio is higher than 0.56.

- (4) The proportion and viscosity of the liquid phase and the activities of PbO and ZnO in the liquid were calculated from FactSage to explain the reduction mechanisms of the lead-rich slags.

### FUNDING

This research received no external funding.

### CONFLICT OF INTEREST

The authors declare that they have no conflict of interest.

### SUPPLEMENTARY INFORMATION

The online version contains supplementary material available at <https://doi.org/10.1007/s11837-022-05413-x>.

### REFERENCES

- H.Y. Chen, A.J. Li, and D.E. Finlow, *J. Power Sources* 191(1), 22–27. (2009).
- X. Zhu, L. Li, X. Sun, D. Yang, L. Gao, J. Liu, and J. Yang, *Hydrometallurgy* 117, 24–31. (2012).
- U.S. Geological Survey. “Mineral commodity summaries 2021” (U.S. Geological Survey, 2021) <https://doi.org/10.3133/mcs2021>.
- L. Chen, T. Yang, S. Bin, W. Liu, D. Zhang, W. Bin, and Li. Zhang, *JOM* 66, 1664. <https://doi.org/10.1007/s11837-014-1057-1> (2014).
- W. Gao, C. Wang, F. Yin, Y. Chen, and W. Yang, *AMR* 581, 904. (2012).
- W. Wu, P. Xin, and J. Wang, The latest development of oxygen bottom blowing lead smelting technology, in *PbZn 2020: 9th International Symposium on Lead and Zinc Processing*. (Springer, Cham, 2020), pp. 327–336.
- W. Li, J. Zhan, Y. Fan, C. Wei, C. Zhang, and J.-Y. Hwang, *JOM* 69, 784. <https://doi.org/10.1007/s11837-016-2236-z> (2017).
- L. Chen, Z. Hao, T. Yang, W. Liu, D. Zhang, Li. Zhang, S. Bin, and W. Bin, *JOM* 67, 1123. <https://doi.org/10.1007/s11837-015-1375-y> (2015).
- K. Upadhyaya, *Metall. Mater. Trans. B* 17, 271. <https://doi.org/10.1007/BF02655074> (1986).
- N.N. Kinaev, E. Jak, and P.C. Hayes, *Scand. J. Metall.* 34, 150. <https://doi.org/10.1111/j.1600-0692.2005.00733.x> (2005).
- B. Zhao, B. Errington, E. Jak, and P. Hayes, *Can. Metall. Quart.* 49, 241. <https://doi.org/10.1179/cm.2010.49.3.241> (2010).
- X. Hou, K.C. Chou, and B. Zhao, *J. Min. Metall., Sect. B: Metall.* 49(2), 201–206. (2013).
- J. Liao, and B. Zhao, *Calphad* 74, 102282. <https://doi.org/10.1016/j.calphad.2021.102282> (2021).
- C. Feng, M. Chu, J. Tang, Y. Tang, and Z. Liu, *Steel. Res. Int* 87, 1274. <https://doi.org/10.1002/srin.201500355> (2016).
- C.W. Bale, E. BÉlisle, P. Chartrand, S.A. Decterov, G. Eriksson, A.E. Gheribi, K. Hack, I.-H. Jung, Y.-B. Kang, J. Melançon, A.D. Pelton, S. Petersen, C. Robelin, J. Sangster, P. Spencer, and M.-A. Van Ende, *Calphad* 54, 35. <https://doi.org/10.1016/j.calphad.2016.05.002> (2016).
- C.F. Dickinson, and G.R. Heal, *Thermochim. Acta* 340, 89. [https://doi.org/10.1016/S0040-6031\(99\)00256-7](https://doi.org/10.1016/S0040-6031(99)00256-7) (1999).
- E. Bidari, and V. Aghazadeh, *Metall. Mater. Trans. B* 46(5), 2305–2314. (2015).
- F. Vegliò, M. Trifoni, F. Pagnanelli, and L. Toro, *Hydrometallurgy* 60, 167. [https://doi.org/10.1016/S0304-386X\(00\)00197-3](https://doi.org/10.1016/S0304-386X(00)00197-3) (2001).
- Mark Pritzker, *Chem. Eng. Sci* 58, 473. [https://doi.org/10.1016/S0009-2509\(02\)00554-7](https://doi.org/10.1016/S0009-2509(02)00554-7) (2003).
- S. He, J. Wang, X. Zhang, and Y. Li, *Nonferrous Metals*. 3, 13–16. (2010).
- L. Yanting, Y. Tianzu, and L. Mingzhou, *Chinese J. Non-ferrous Metals* 30(5), 1110–1118. (2020).
- G. Pi, and Z. Jia, *Nonferrous Metals*. 6, 17–19. (2009).
- J. Wang, Y. Dong, and G. Feng, *Eng. Sci.* 7, 256–259. (2005).
- H. Kim, H. Matsuura, F. Tsukihashi, W. Wang, D.J. Min, and I. Sohn, *Metall. Mater. Trans. B* 44(1), 5–12. (2013).

**Publisher's Note** Springer Nature remains neutral with regard to jurisdictional claims in published maps and institutional affiliations.